Available online at www.sciencedirect.com
ScienceDirect
Journal of Nuclear Materials 366 (2007) 87–98
journal of nuclear materials
www.elsevier.com/locate/jnucmat

Fracture properties of sintered UO_2 ceramic pellets with duplex microstructure

K. Kapoor *, Ansar Ahmad, A. Laksminarayana, G.V.S. Hemanth Rao

Quality Assurance Group, Nuclear Fuel Complex, Hyderabad 500 062, India

Received 11 September 2006; accepted 12 December 2006

Abstract

The fracture behavior of sintered ceramic UO_2 material is studied in light of microstructural (grain size and porosity) parameters. Using Vicker's indentation technique the fracture properties have been evaluated and compared for different microstructural conditions present in the same sample. In a sintered pellet sample, duplex microstructure was obtained by addition of additives like SiO_2 and Fe_2O_3. The duplex microstructure consisted of (1) high-density region with fine intragranular porosity present in coarse sized grain and (2) low-density region having intragranular porosity with fine grain size. The fracture toughness in the low-density region was higher as compared to the high-density region. This was attributed to crack tip deflection and branching at the grain boundary due to porosity. Acoustic emission signals were obtained during indentation. These were used to characterize the crack initiations and propagation during indentation. Toughening due to porosity with fine grain size has been explained using a mathematical model. These observations are in line with the observations of a tough rim structure formed at high burn-up. The rim has similar microstructural features to those observed in the low-density region of the sample used in the current study. In the end it is concluded that toughening in these ceramics can be achieved by suitable control of porosity and microstructure.

1. Introduction

The fracture properties of sintered UO_2 pellets are of significance both during manufacture of the pellets and in the in-pile behavior. Improvement in the fracture properties would yield chipping resistance while handling and grinding of pellets during manufacture. In the in-pile behavior, the radial cracking of pellets at high burn-up is a source of release of fission gas from the pellets. Retaining fission gas in the pellets is of an advantage, as this would reduce pellet-clad chemical interaction which could otherwise lead to intergranular stress corrosion cracking of the clad material. Thus, microstructure having inherent resistance towards the radial cracking could improve the performance of the fuel pin under irradiation.

In case of Pressurised Heavy Water Reactor (PHWR), the natural UO_2 pellets are made to density within the range of 95–98% of TD (TD refers to the theoretical density of $UO_2 = 10.96$ g/cc). In

* Corresponding author. Tel.: +91 40 27184091; fax: +91 40 27121271.
E-mail address: kapoork@nfc.ernet.in (K. Kapoor).

0022-3115/$ - see front matter © 2007 Published by Elsevier B.V.
doi:10.1016/j.jnucmat.2006.12.044

conventionally sintered UO_2 pellets with density in this range, the porosity is distributed uniformly within the grains. At lower density than 95% TD, the thermal conductivity of the pellets would reduce to undesirable value, which could increase pellet centerline temperature, and ultimately increase the fission gas release. But, a small quantity of pores is useful to trap the fission gases effectively, and hence a minimum porosity is specified (density exceeding 98% TD being unacceptable). With this limitation of total pore volume allowed in the sintered pellets, we designed a microstructure with redistribution of the pores from random distribution to network porosity. In this structure there were grains nearly free of porosity, surrounded by grains with high porosity (porosity envelop) and having fine grain size. In this work, such a structure has been denoted as a duplex microstructure. The fracture properties of such a microstructure has been evaluated and compared with the conventional pellet microstructure with uniformly distributed intragranular porosity.

The microstructure of the high burn-up pellets consists of a rim, which is formed after intense irradiation [1,2]. The mechanical properties in the rim region of the pellet are characteristically different from that of the core of the pellet [2]. This difference in the mechanical properties of the rim region has been attributed to the high porosity and the fine recrystallised grain size existing in this region. The schematic microstructure in the rim and the surrounding region is shown in Fig. 1. The microhardness and the fracture toughness measured using Vicker's hardness technique as a function of radial distance. The porosity and pore density in the rim region increases exponentially towards the pellet edge (maximum of 15%) with a corresponding increase in the fracture toughness measured in terms of K_{1C} (plane-strain fracture toughness). These results indicate that the fracture toughness of the ceramic UO_2 material has a strong dependence on the microstructure parameters like porosity and grain size. These parameters could then be used for microstructure design to resist fracture in the ceramic UO_2 material. With this objective a microstructure with features similar to rim structure was synthesized in the as-sintered UO_2 pellets and evaluated for fracture properties. The influence of the grain size and the pore size on the fracture properties has been studied in case of ZnO by Lu et al. [3]. It is reported that although mechanical properties including elastic modulus, strength, and toughness usually decreased with increasing porosity in brittle materials, but due to defect–microstructure interaction when the density of porosity is high, the fracture toughness behavior in rather complex in nature and does not follow the expected trend. The influence of grain size on fracture behavior of brittle ceramics has been studied by Zimmermann and others [4–6]. It is reported by them that grain size had a clear effect on fracture strength of ceramics. For a coarse-grained material, the fracture strength increased with decreasing grain size. Conversely, for the fine-grained materials, fracture strength increased only slightly or remained constant with decreasing grain size. Pore size, shape effects and pore location, were shown to affect strength and fracture properties when pore sizes are of the order of the grain size [7]. From the above discussion it is clear that the porosity size, location and relation with grain size are key parameters for fracture behavior of ceramics. In the present case, we try to analyze three cases

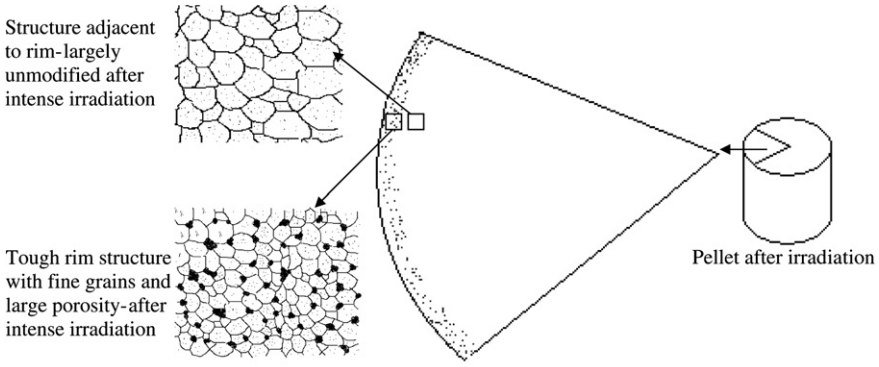

Fig. 1. Schematic rim structure formed after irradiation showing a fine rim region having fine grain size and coarse porosity. The adjacent region retains the original structure with low porosity and coarser grain structure.

where microstructure–porosity interaction leads to complex fracture behavior.

1.1. Measurement of fracture toughness of ceramic materials

After early work of Palmqvist in 1957 [8] it was recognized that the surface radial cracking due to a sharp indentation as an indicative of the fracture toughness of the material, the Vickers indentation test has been widely adopted for fracture toughness determination for brittle materials, particularly glasses and ceramics. Consequently, numerous semi-empirical equations relating material fracture toughness to the measured indentation parameters, such as the applied indentation load, final radial crack length, or indentation impression size, have been derived based on experimental observations and/or theoretical considerations [9,10]. Fig. 2 shows a schematic diagram showing the location of cracks at the edges of Vickers indentation. The indentation cracks in case of sintered UO_2 pellet in the present study are also shown.

Among the existing indentation fracture mechanics models for the well-developed half-penny crack, the Lawn–Evans–Marshall (LEM) model [11] has the feature that the complex elastic–plastic indentation stress field is resolved into a reversible elastic component and an irreversible residual component. The elastic component is taken to operate outside the plastic zone, reaching its maximum intensity on full loading and reversing completely on unloading. The residual component is derived from the wedging action of the deformation zone, also reaching its maximum at full loading but persisting as the indenter is removed, providing the primary driving force for the half-penny crack configuration in the final stage

$$K_c = \delta\left(\frac{E}{H_0}\right)^{1/2}\frac{P}{c^{3/2}}, \tag{1}$$

where P is the applied indentation load, c is the half-length of the half-penny crack, E is Young's modulus, H_0 is the apparent hardness defined as the ratio of the applied indentation load to the projected area of the resulting indentation impression, and δ is a non-dimensional constant that is primarily a function of the indenter geometry. The constant δ is generally regarded as a material independent constant and its value for the standard Vickers indenter has been established by calibration with known fracture toughness values on a variety of ceramics. For example, Lawn et al. [11] obtained $\delta = 0.014$; Anstis et al. [12] obtained $\delta = 0.016 \pm 0.004$.

1.2. Acoustic emission for characterization of the fracture behavior

During indentation there are three stages namely, loading, dwell and unloading. During the loading process the penetration is accompanied by strong acoustic signals due to crack initiation, which is

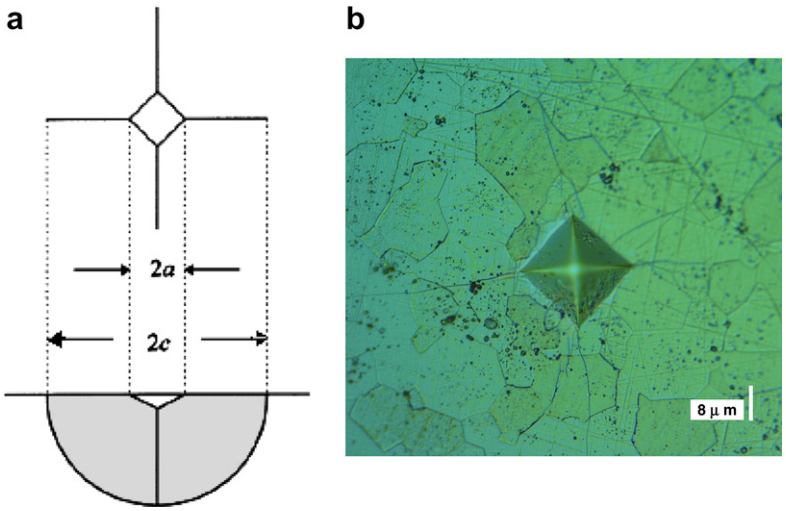

Fig. 2. (a) Schematic diagram showing the location of cracks at the edges of Vickers indentation. These surface cracks are in the form 'half-penny' shape. (b) Indention cracks in UO_2.

followed by secondary signals arising due to crack propagation, which may extend during the dwell period. The crack formation during the indentation generates a burst signal, which can be picked up by a probe attached to the sample itself. Acoustic emission (AE) is equally sensitive to the surface and sub-surface cracks formed during indentation. The nature of cracking is characterized by AE parameters like ring-down counts, peak-amplitude, energy, etc. In order to have an insight of the fracture process in the sample with duplex microstructure, the AE signatures during the indentation at different regions were compared. Also the variation in the AE with applied load during indentation was recorded.

2. Synthesis of pellets with duplex microstructure

Certain additives like SiO_2 or silicates of other oxides ($Fe_2O_3 + SiO_2$) when added in very small quantity to the UO_2 powder before pressing to green pellets lead to reduction in the sintered density. At high sintering temperature these additives (SiO_2, or $Fe_2O_3 + SiO_2$) volatilize and leave behind porosity. This behavior was used to generate the required duplex microstructure in the sintered pellets. In the present case, these additives (SiO_2, Fe_2O_3 and $Fe_2O_3 + SiO_2$) were not added directly to the fine powder, instead the powder was first granulated (pre-compacted at 75–100 MPa) and then these additives were added. The granules with added additives were thoroughly mixed to coat the granules with these additives. In such a condition the cores of such granules were free from these additives, while the surfaces were coated with additives. The content of additives (Fe, Si) was varied from 0.1 to 0.5 wt%. When both the additives were added (Fe + Si) the total content was varied from 0.2 to 0.8 wt%. Table 1 gives the details of the quantity of additives added to the granules. The coated granulated material was compacted to cylindrical pellets using a hydraulic press at a pressure of 250–300 MPa. Soaking at intermediate temperature (1300–1500 °C) for 8 h and at high temperature of 1700 °C for 8–10 h was done during sintering. Table 1 shows the effect of sintering on removal of volatile additives. The measured sinter density and the residual impurity content after sintering is given in Table 1. Out the three cases (Fe_2O_3 alone, SiO_2 alone and $Fe_2O_3 + SiO_2$) there was no change in the sinter

Table 1
Effect of addition of SiO_2, Fe_2O_3 and $SiO_2 + Fe_2O_3$ on the sinter density, also the green density of the pellet before sintering and residual Fe and Si content after the sintering cycle are reported

SNO	G.D.	S.D.	R.A.	SNO	G.D.	S.D.	R.A.	SNO	G.D.	S.D.	R.A.
A (SiO_2 – 0.1%)				*B (SiO_2 – 0.2%)*				*C (SiO_2 – 0.5%)*			
1	5.73	10.64	Si < 30	1	5.66	10.55	Si < 30	1	5.52	10.41	Si < 30
2	5.71	10.68	Fe 15	2	5.65	10.53	Fe 48	2	5.56	10.41	Fe < 10
3	5.71	10.66		3	5.66	10.55		3	5.56	10.45	
4	5.68	10.63		4	5.69	10.58		4	5.56	10.41	
5	5.67	10.64		5	5.64	10.55		5	5.54	10.41	
6	5.69	10.68	O/U = 2.006	6	5.66	10.53	O/U = 2.007	6	5.58	10.40	O/U = 2.013
D (Fe_2O_3 – 0.1%)				*E (Fe_2O_3 – 0.2%)*				*F (Fe_2O_3 – 0.5%)*			
1	5.68	10.65	Si < 30	1	5.68	10.63	Si < 30	1	5.69	10.67	Si < 30
2	5.70	10.68	Fe 27	2	5.71	10.71	Fe 31	2	5.71	10.68	Fe 25
3	5.70	10.69		3	5.70	10.71		3	5.67	10.63	
4	5.68	10.69		4	5.71	10.67		4	5.64	10.62	
5	5.70	10.70		5	5.73	10.69		5	5.65	10.64	
6	5.73	10.68	O/U = 2.004	6	5.64	10.67	O/U = 2.004	6	5.67	10.63	O/U = 2.005
G (Fe_2O_3 + SiO_2) – 0.2%				*H (Fe_2O_3 + SiO_2) – 0.5%*				*I (Fe_2O_3 + SiO_2) – 0.8%*			
1	5.66	10.64	Si < 30	1	5.63	10.57	Si < 30	1	5.57	10.50	Si < 30
2	5.72	10.67	Fe 27	2	5.63	10.59	Fe 20	2	5.54	10.48	Fe 25
3	5.64	10.66		3	5.60	10.58		3	5.53	10.45	
4	5.69	10.69		4	5.61	10.52		4	5.57	10.49	
5	5.69	10.68		5	5.61	10.57		5	5.55	10.49	
6	5.65	10.67	O/U = 2.004	6	5.63	10.58	O/U = 2.004	6	5.53	10.43	O/U = 2.003

G.D.: green density, S.D.: sinter density, R.A.: residual additive (analysis after sintering).

density only in the case when Fe_2O_3 was added alone. Fig. 3 gives the microstructures of the sintered pellets with different additives added at the granule stage. It was observed that Fe_2O_3 (when added alone up to a content of 0.5 wt%) does not yield a duplex structure (Fig. 3(a)–(c)). SiO_2 added alone (Fig. 3(d)–(f)) or with Fe_2O_3 (Fig. 3(g)–(i)) resulted in strong duplex structure. The duplex structure consists of grains with high porosity and low grain size (~10 μm) at the prior granule boundary. This is evident from the high magnification microstructures shown in Fig. 3(j) and (k). There is a band of higher porosity region, as seen in Fig. 4. Within this region there is fine grain size and higher porosity. The porosity is either coarse-and-rounded (seen in Fig. 4(a)), or is present as a channel surrounding the grains (marked in Fig. 4(b)). No such channel type or intergranular type porosity is present in the high-density region of the pellet (seen in Fig. 4(c)). The porosity observed in the micrograph Fig. 4(a) and (b) is due to the additives which influence sintering in the local region. At the intermediate stage of sintering as the temperature reaches above the melting point of SiO_2, these additives volatilize through the grain boundary channels leaving behind porosity at the grain boundary. The porosity present at the grain boundary restricts grain coarsening by obstruction of grain boundary migration during the end stage of sintering. The fine grain size observed in this region appears to be an effect of porosity present at the grain boundary.

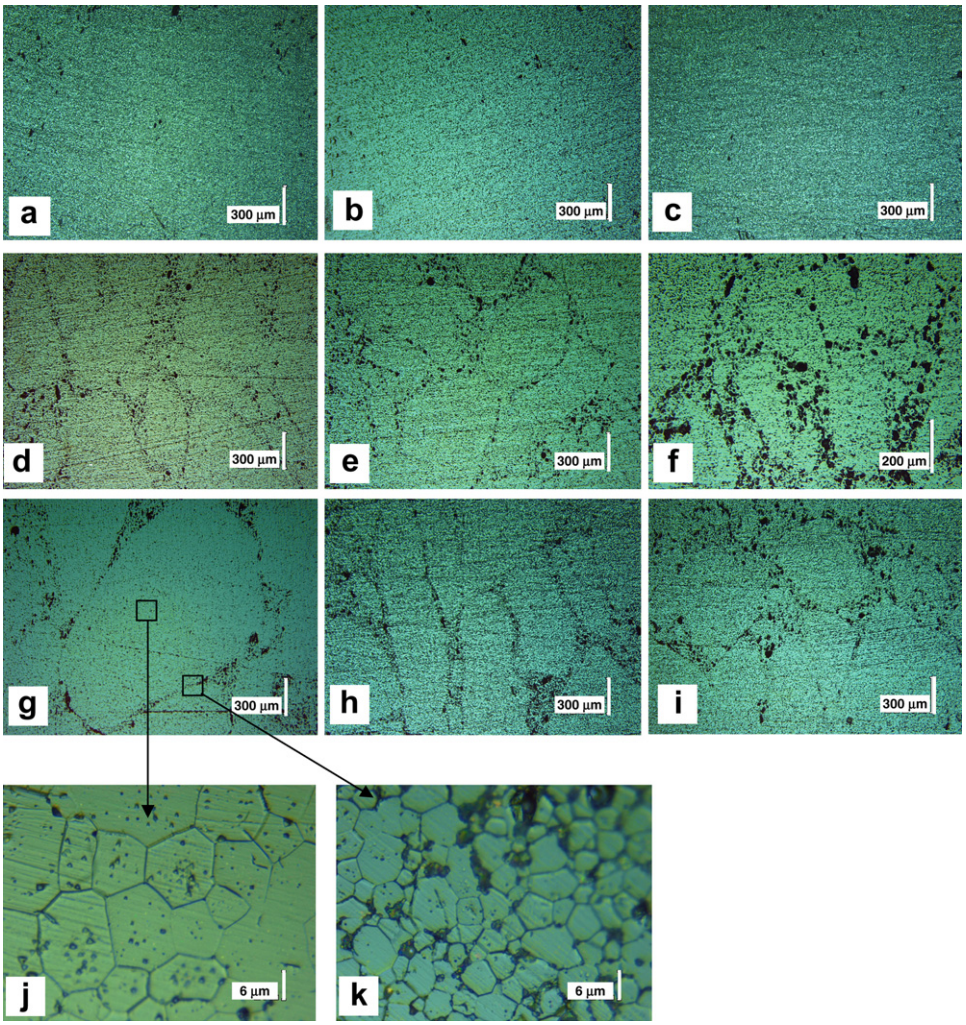

Fig. 3. Influence of additives in different amounts on the microstructure, Fe_2O_3 – 0.1, 0.2 and 0.5 wt% (a)–(c), SiO_2 – 0.1, 0.2 and 0.5 wt% (d)–(f), $Fe_2O_3 + SiO_2$ – 0.2, 0.5 and 0.8 wt% (g)–(i), the magnified regions in (g) showing duplex structure is shown in (j) and (k).

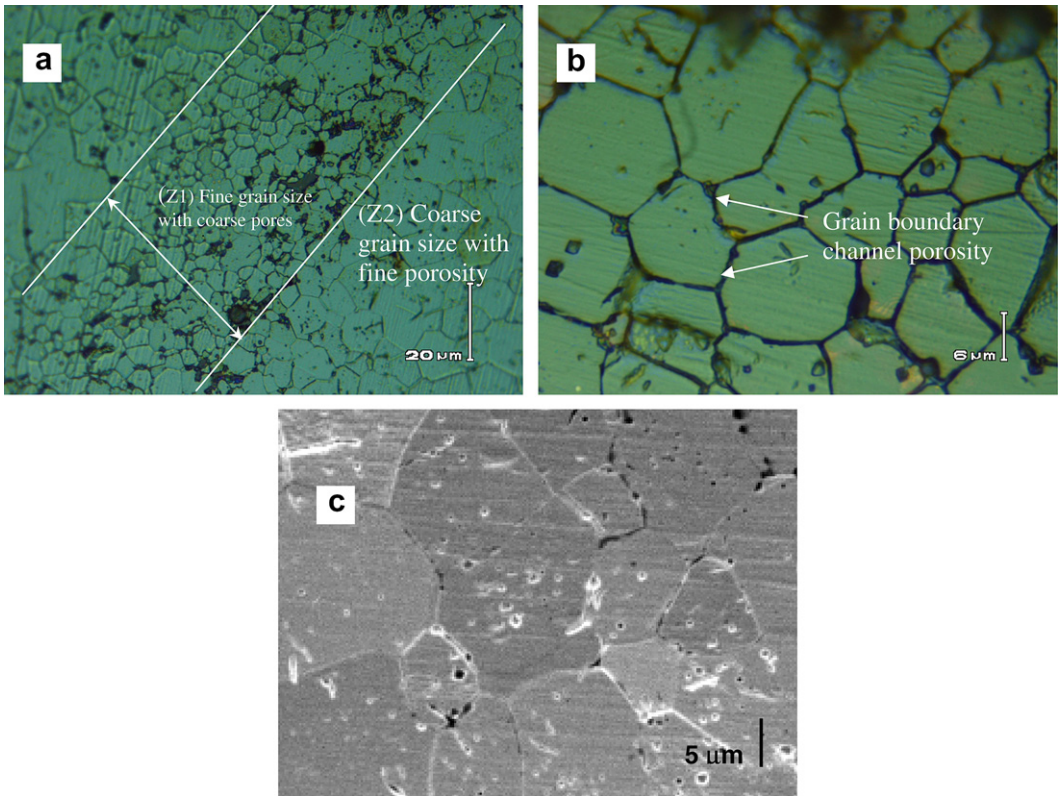

Fig. 4. (a) Microstructure at the prior granule boundary (Z1) and adjacent to it (Z2). In the boundary region coarse and rounded porosity exists in addition to channels of porosity at the grain boundary as seen in (b). The surrounding high-density region (Z2) in (c) shows coarse grain size and no channel type porosity.

3. Experimental

The measurement of the Vicker's hardness was carried out using 1000 g load and the lengths of the diagonals and cracks at the edge of the Vickers indentation were measured. The indentation loading time was 7 s followed by dwell period of 15 s. From the length of the cracks and the indentation hardness the fracture toughness was calculated using the Lawn–Evans–Marshall (LEM) approach [11] as mentioned above. The microstructure was evaluated in the as-sintered stage for all the additives using optical microscopy. For obtaining AE signals during the indentation, a probe with 150 kHz resonant frequency with a pre-amplifier having gain of 40 dB was used to acquire the AE signals. The bottom flat surface of the sample was coupled to the AE probe and held firmly with grips lined with rubber to avoid spurious noise during indentation. A PAC (Physical Acoustic Corporation, USA) model LOCAN 320 AE unit was used to acquire in real time signals and the same were analyzed in time domain.

4. Results

4.1. Microstructure and sinter density upon addition of additives to granules

By addition of Fe_2O_3 to UO_2 up to 0.5 wt% the following observations were made. There was a formation of a metallic phase as seen in Fig. 5. No distinct prior granule boundary was observed and no duplex microstructure is observed. The sintered density after addition of Fe_2O_3 up to 0.5 wt% is not affected as seen from Table 1.

By addition of SiO_2 addition to UO_2 up to 0.5 wt% the following observations were made. Grain boundary channel type porosity is observed. In addition to the channel type porosity there is large size porosity in this region. Fine sized grains are formed at the prior granule boundary (duplex grain size). Sinter density is affected by addition of SiO_2, as seen from Table 1. There is a reduction in the sinter density up to 10.40 g/cc with addition of 0.5% SiO_2.

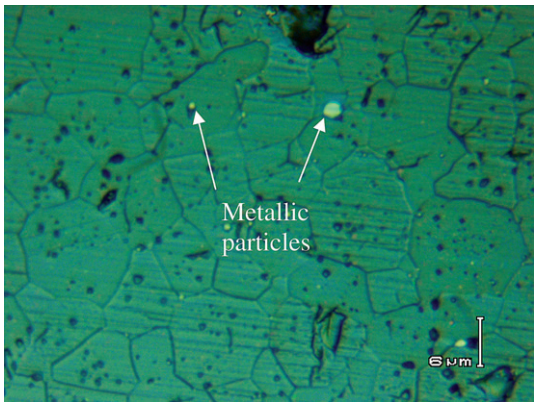

Fig. 5. Microstructure of the sample with Fe_2O_3 addition showing presence of shining metallic phase in the microstructure.

By addition of $Fe_2O_3 + SiO_2$ to UO_2 up to 0.8 wt% the following observations were made. The grain size at the granule boundary is fine leading to duplex grain size in the pellet. There is a formation of grains with high pore size along with channel type porosity at the grain boundary (duplex pore density). There is no metallic (Fe) phase present and the sinter density is not affected as much as with addition of SiO_2 alone as seen from Table 1.

4.2. Fracture behavior

The fracture toughness was calculated from the crack length after indentation of the samples. The results of the measurement are reported in Table 3. It is observed that the indentation in the low-density region of the pellet with duplex structure is in the range of 2.2–5.1 MPa $\sqrt{m}$, while in case of high-density region the toughness is much lower in the range of 0.2–0.45 MPa $\sqrt{m}$. For comparison purpose, Fig. 6(a) shows the indentation cracks in the two nearby regions having different microstructure. In Fig. 6(b) and (c) the selected areas are magnified to show the nature of crack propagation. In

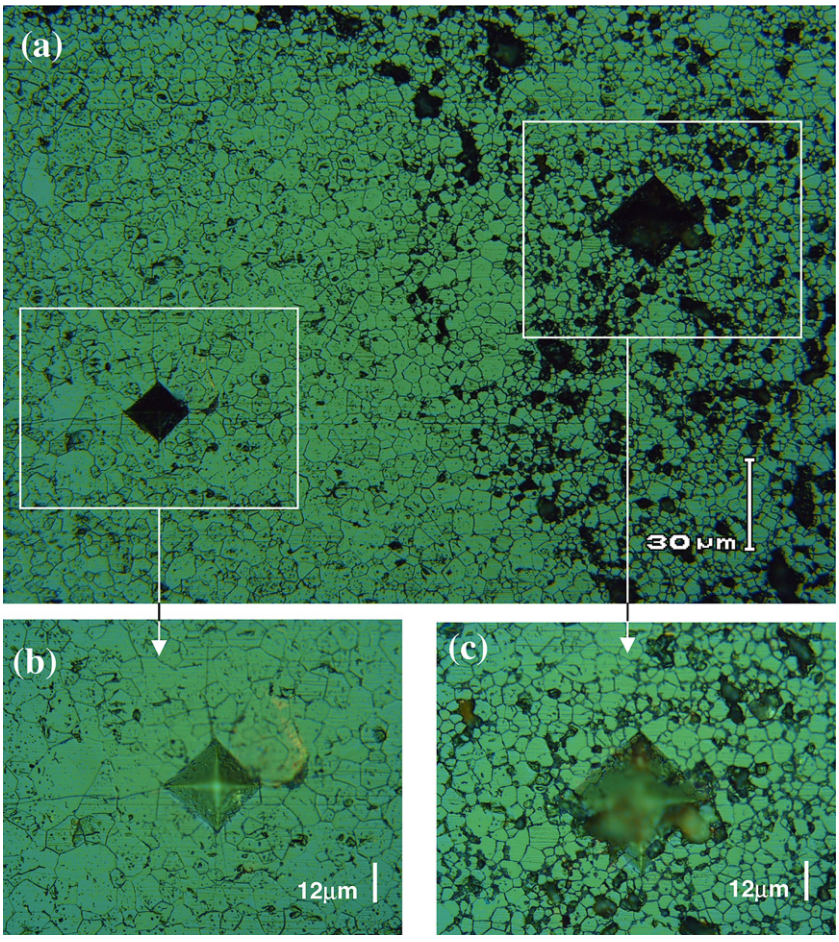

Fig. 6. Vicker's indentations and cracks in the two regions with duplex microstructure.

case of Fig. 6(b) the crack propagates freely through the grains (transgranularly), also the indentation size is smaller leading to higher hardness (see Table 3). In the second case Fig. 6(c) the crack propagation is restricted and the indentation size is much larger with corresponding hardness much lower. The low hardness in this case is related to higher porosity in this region, which leads to lower load carrying capacity. For explanation of the observation of higher toughness in this region, there appears a significant difference in the crack path at the tip of indentation, which is explained in detail in a later section.

4.3. AE during indentation

The AE signals obtained during indentation with load in a high-density location from 200 to 1000 g are given in Fig. 7(a)–(d). The AE signals were also obtained with indentation using 1000 g load in a nearby low-density region Fig. 7(e). It was observed that the ring-down counts are a good measure of the AE activity during indentation. There was a characteristic difference in the AE obtained during indentation at low-density and high-density regions of the sample. Comparing Fig. 7(d) and (e) it is observed that as the indenter was loaded against the sample there was a strong signal, followed by a strong signals in case of Fig. 7(d) and very feeble signals in case of Fig. 7(e) extending unto dwell period. Those signals, which follow instantly, are likely from the indenter penetration and crack initiation. Further acoustic activity in the dwell time by extension of these cracks is likely through the elastic release of residual stress developed during indentation.

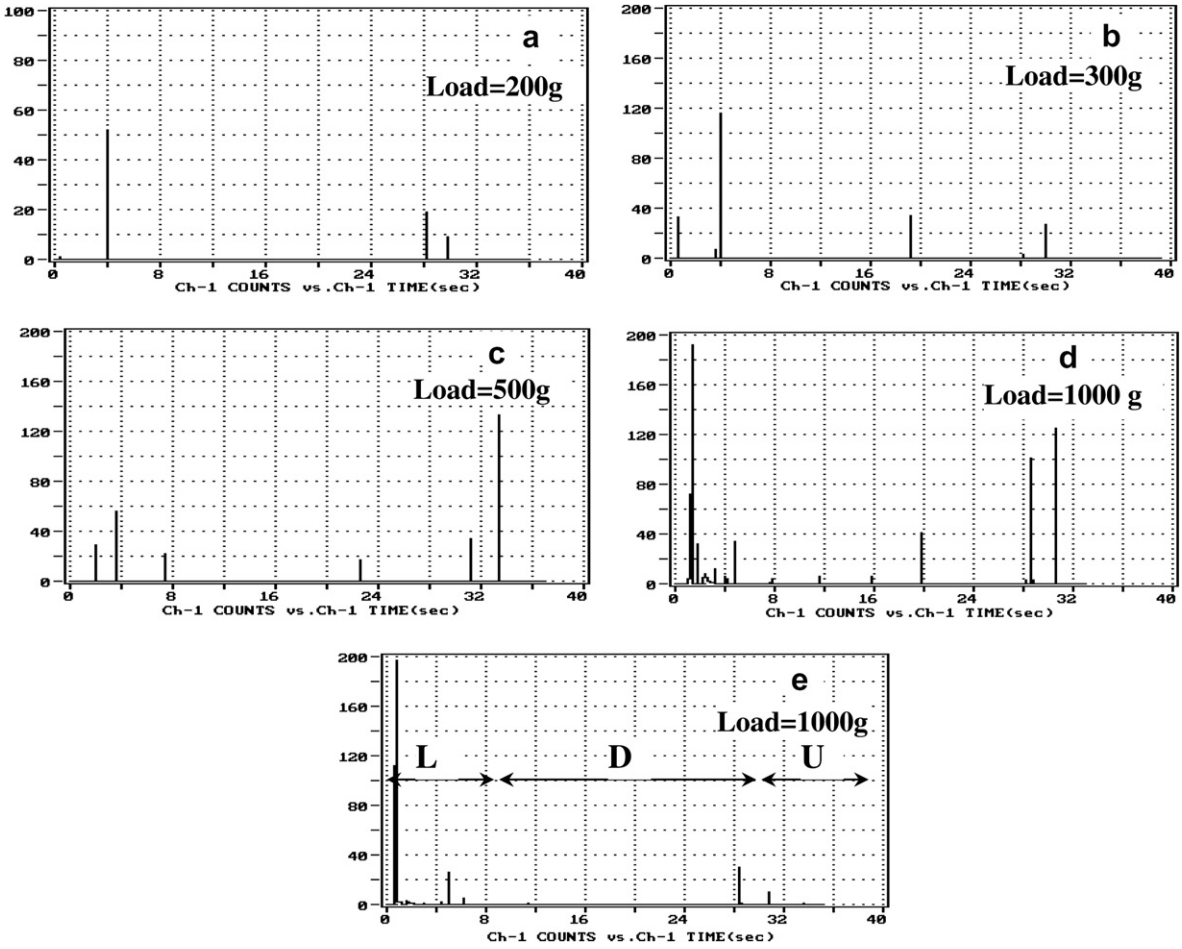

Fig. 7. AE during indentation, plots of AE parameter – ringdown counts as a function of time elapsed during indentation (L = loading, D = Dwell and U = Unloading). (a)–(d) load as 200 g, 300 g, 500 g and 1000 g, respectively at high-density location and (e) 1000 g load at low-density region.

5. Discussion

5.1. Fracture, microstructure and porosity relationships

The fracture process zone ahead of the indentation tip shows different characteristic features in the two regions. Fig. 8 shows that in case of zone with high porosity and lower grain size the there is a higher resistance to crack propagation either by blunting by large porosity (Fig. 8(a)) and or by crack front deflection at the grain boundary (Fig. 8(b)). It is observed that the transgranular crack propagation is rather easy in a region with fine intragranular porosity and higher grain size (Fig. 8(c)). In case of indentation within a high porosity region (Fig. 8(a)), the crack is intercepted by large size porosity and its growth is hampered by blunting and ridge formation (known as hackle a region). Alternatively, in the second case (Fig. 8(b)), the crack propagates through the grain boundary channel porosity leading to a crack deflection. In case of indentation at a high porosity region, the crack extends only to a few grains. In contrast to this in case of indentation at a low porosity region, the crack moves freely through the grains (transgranular) and the crack length in this case is several times the grain diameter. Thus there seem to be a certain toughening in the regions with high porosity; it is intended here to explain this behavior. There are three possibilities of crack propagation are tabulated in Table 2 which are discussed in the following section. It is attempted to explain and correlate the fracture behavior with the microstructure and porosity using mathematical models.

For a generalized case the stress required for fracture σ is given by

$$\sigma = \frac{\pi}{2} \cdot \left(\frac{\beta}{\tan\beta}\right)^{1/2} \cdot \frac{\sigma_p}{\sigma_c} \cdot \left(\frac{E\gamma}{R+L}\right), \tag{2}$$

where E is the Young's modulus, γ is the fracture energy , $\beta = (\pi R/2R + \lambda)$, $R =$ porosity size, $\lambda =$ spacing between the porosity, $L =$ crack length, $G =$ average grain size, σ_p/σ_c is the ratio of the stress

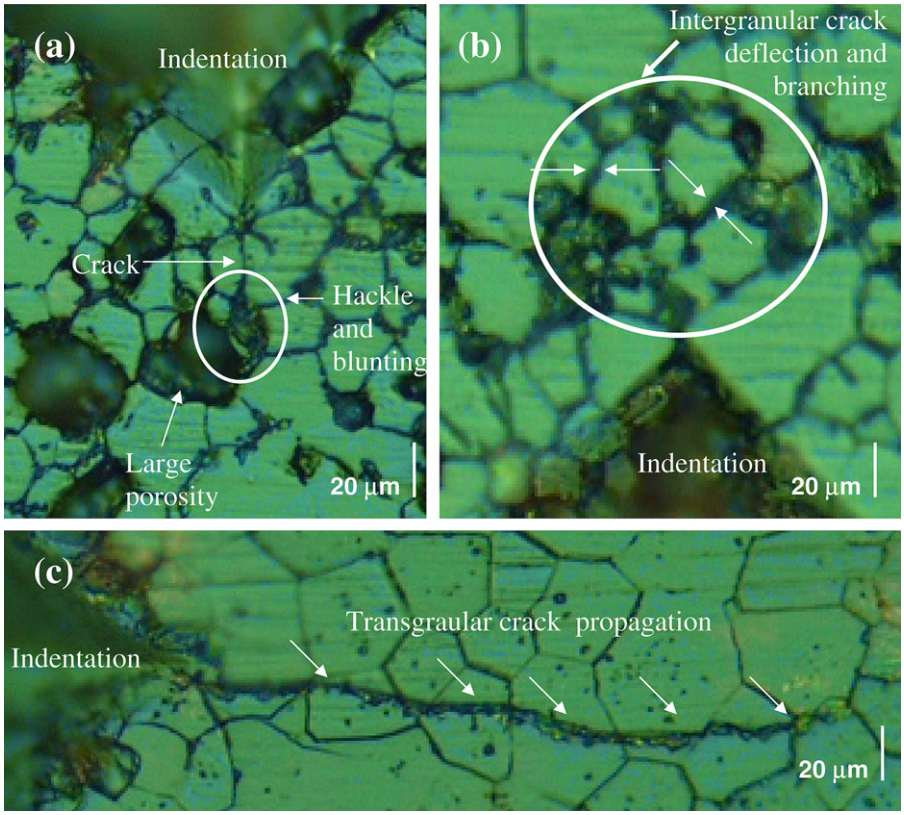

Fig. 8. Crack propagation at the tip of indentation in different regions of samples. (a) Region with large size porosity (nearing to grain size) and low grain size, (b) region with grain boundary channel porosity and low grain size, (c) region with fine intragranular porosity and higher grain size.

Table 2
Cases for microstructure–porosity influence on the fracture properties

Case	Porosity character	Microstructure features	Fracture after indentation	Crack length after indentation	Figure
1	Fine intragranular porosity	Coarse Grain size	Transgranular	10–20 grains – no branching	Fig. 8(c)
2	Large rounded porosity	Fine Grain size	Transgranular	Few (3–4) grains branching	Fig. 8(a)
3	Grain boundary channel type porosity	Fine grain size	Intergranular	Few (3–4) grains branching	Fig. 8(b)

to propagate a single pore-crack combination to the stress to propagate a crack of dimensions $R + L$.

Case 1: Fig. 9(a) depicts the such case where $R < L$, $L \gg G$ and $\lambda/R > 1$,

$$\sigma = Y\left(\frac{E\gamma}{L}\right)^{1/2}. \tag{3}$$

For such a case, the above relationship holds good for the conditions mentioned above, the stress required fracture is related through the grain size G which in this case is coarse and $L \gg G$, the fracture stress is low.

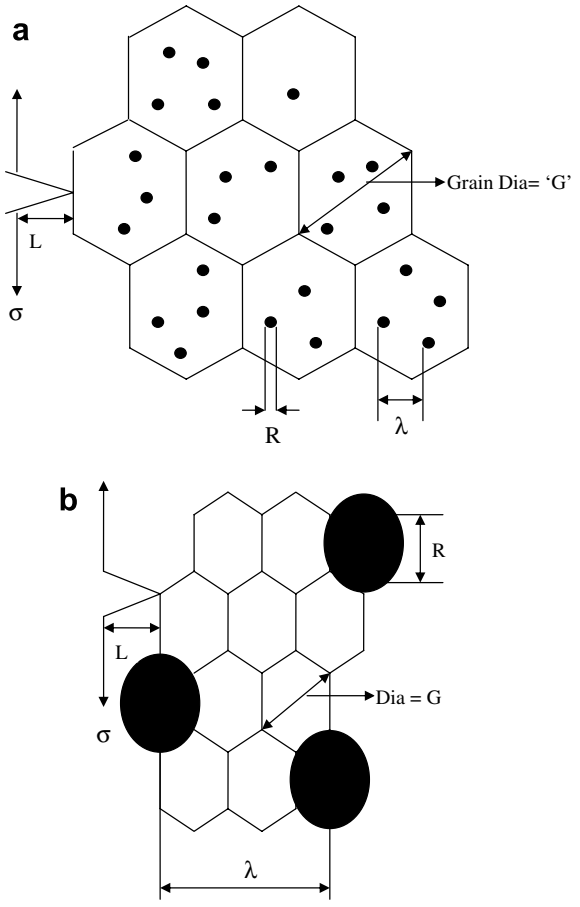

Fig. 9. (a) Case 1 with fine rounded intragranular pores and coarse grain size and (b) case 2 with large rounded pores and fine grain size.

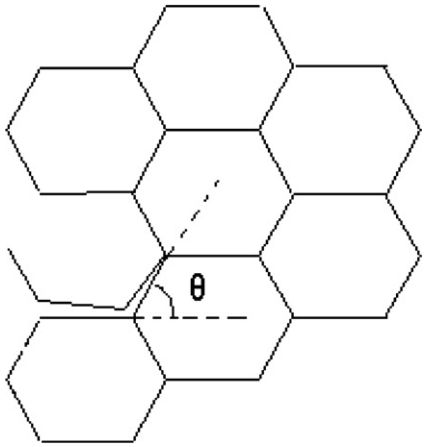

Fig. 10. Crack deflection at grain boundary by angle θ.

Table 3
Microhardness measured in the low-density (LD) and high-density (HD) regions of the samples A to I identified in Fig. 3 having history given in Table 1

Sample	Region	Microhardness (kg/mm^2)	Fracture toughness K_{1C} (MPa $\sqrt{m}$)
A	LD	529	2.209
	HD	564	0.205
B	LD	540	3.416
	HD	604	0.376
C	LD	350	5.075
	HD	566	0.298
D	HD[a]	599	0.313
E	HD[a]	654	0.216
F	HD[a]	640	0.444
G	LD	496	5.00
	HD	571	0.356
H	LD	532	2.799
	HD	578	0.359
I	LD	555	4.846
	HD	613	0.231

[a] No low-density region in these samples (refer Fig. 5).

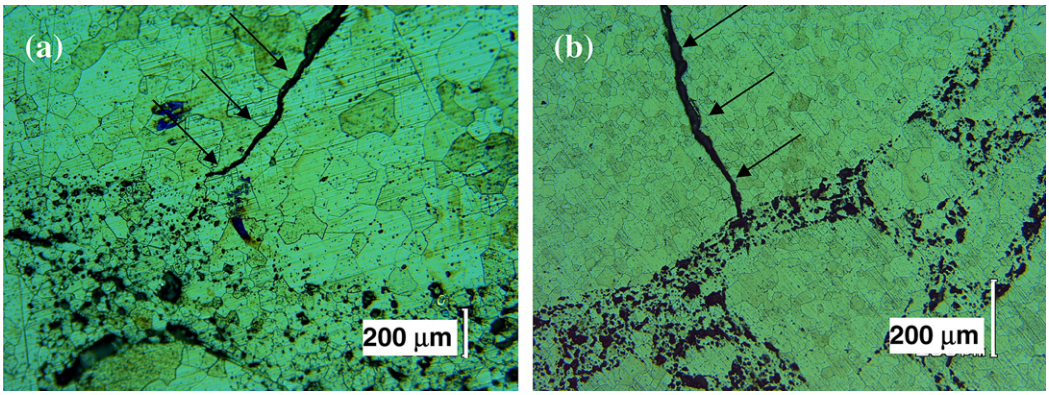

Fig. 11. (a) and (b) two different locations in the pellet with cracks (see arrows) being seen as arrested at the high porosity regions.

Case 2: Fig. 9(b) depicts the case where $R \approx L$ and $L \approx G$, the relationship is given by

$$\sigma = Y\left(\frac{E\gamma}{R+L}\right)^{1/2}. \tag{4}$$

Here due to fine grain size the fracture stress is high. It is clear from the above discussion that there exists an influence of the grain size with microporosity on the fracture properties.

Case 3: The mechanism proposed for this toughening is due to crack deflection at the grain boundary, which is illustrated in Fig. 10. On deflection to the grain boundary, the average stress intensity at the crack tip (K_{tip}) is reduced, as the applied stress is no longer always normal to the crack plane. The applied stress intensity (K_{app}) is related to the K_{tip} by the following relationship:

$$K_{tip} = (\cos^3\theta/2)K_{app}, \tag{5}$$

where θ is the angle of deflection defined by Fig. 10. Based on this equation and assuming average θ values of, say, 45°, the increase of the fracture toughness shall be 1.25 times by this mechanism. But, on comparing this conclusion with the experimental results listed in Table 3, it is clear that crack deflection by itself accounts for some of, but not all, enhanced toughening. The other possible mechanism is crack bifurcation around the grains through the grain boundary porosity channels. In this process the crack is likely to interact with the porosity channels observed at the grain boundary in case of low-density regions. These channels could provide greater crack opening displacement and observed toughening.

In the present case looking at a cross-section, there are layers of high porosity regions, but these layers are not continuous hence such a duplex structure can also be called a pseudo-layered structure. Ceramic layered systems have attracted wide attention in recent years as such configurations have shown to be effective in improving the toughness of the ceramic components [13,14]. It is noted that such enhancement in fracture properties is mainly attributed to the crack deflection capability in the interlayers of such systems [15,16]. The effect of a porous interlayer on crack deflection in ceramic laminates was demonstrated by Ma et al. [17]. They have shown that the pore interaction effect in the porous interlayer cannot be neglected. It is also shown that an increase of porosity in the porous interlayer promotes crack deflection, and hence can improve fracture toughness of the system. In the present case, the crack branching through the grain boundary in the porous pseudo-interlayers could be a toughening mechanism. To verify this a simple test was conducted. Large sized cracks were generated in pellets with duplex structure by rapid thermal cooling. The large sized cracks are seen in Fig. 11 due to this effect. On careful observation it is noted that these cracks were arrested at the high porosity layers, suggesting toughening by the duplex microstructure.

6. Conclusions

1. The influence of microstructure, namely the porosity character and the grain size, has been studied on the fracture properties of sintered ceramic UO_2 pellets.
2. Using the pellet with duplex structure, in the low-density region with fine grain size, the crack deflection and branching at the grain boundary resulted in higher toughness. In the high-density region with coarse grain size, the crack propagation was transgranular and produced lower toughness.

The low-density region was softer as compared to the high-density region due to lower load carrying capacity.

3. Crack initiation and growth on indentation is accompanied by acoustic signals. These were analyzed for crack initiation and propagation in the two regions.
4. The toughening in the low-density region was associated with crack fronts being deflected to the grain boundary where porosity channels were present leading to tortuous crack propagation. Such toughening effects have also been observed in the rim structure in high-irradiated UO_2 pellets and in ceramic laminates.
5. Pellets with duplex microstructure were resistant to cracking due to rapidly cooling (thermal shocks) due to inherent high toughness.

Acknowledgements

The authors respectfully dedicate this work to the late R.K. Srivastava, Ex. Deputy Chief Executive, QA Group, NFC. The authors gratefully acknowledge the encouragement from Mr R.N. Jayaraj, Chief Executive, NFC and kind permission to publish this work.

References

[1] Hi. Matzkc, J. Spino, J. Nucl. Mater. 248 (1997) 70.
[2] J. Spino, K. Vennix, M. Coquerelle, J. Nucl. Mater. 231 (1996) 79.
[3] Chunsheng Lu, Robert Danzer, Franz Dieter Fischer, J. Eur. Ceram. Soc. 24 (2004) 3643.
[4] A. Zimmermann, M. Hoffman, B.D. Flinn, R.K. Bordia, T.-J. Chuang, E.R. Fuller Jr., et al., J. Am. Ceram. Soc. 81 (1998) 2449.
[5] A. Zimmermann, J. Rödel, J. Am. Ceram. Soc. 81 (1998) 2527.
[6] A. Zimmermann, J. Rödel, J. Am. Ceram. Soc. 82 (1999) 2279.
[7] R.W. Rice, Mater. Sci. Eng. Al 12 (1989) 215.
[8] S. Palmqvist, Jernkontorets Ann. 141 (1957) 303 (in Swedish).
[9] C.B. Ponton, R.D. Rawlings, Mater. Sci. Technol. 5 (1989) 865.
[10] M. Sakai, R.C. Bradt, Int. Mater. Rev. 38 (1993) 53.
[11] B.R. Lawn, A.G. Evans, D.B. Marshall, J. Am. Ceram. Soc. 63 (1980) 574.
[12] G.R. Anstis, P. Chantikul, B.R. Lawn, D.B. Marshall, J. Am. Ceram. Soc. 64 (1981) 533.
[13] W.J. Clegg, K. Kendall, N.M. Alford, J.D. Birchall, T.W. Button, Nature 347 (1990) 455.
[14] K.S. Blanks, A. Kristoffersson, E. Carlstrom, W.J. Clegg, J. Eur. Ceram. Soc. 18 (1998) 1945.
[15] W. Lee, S.J. Howard, W.J. Clegg, Acta Mater. 44 (1996) 3905.
[16] W. Lee, W.J. Clegg, The deflection of cracks at interfaces, in: T.W. Clyne (Ed.), Key Engineering Materials, vols. 116&117, Trans Tech. Publications, Aedersmannsdorf, Switzerland, 1996, p. 193.
[17] J. Ma, Hongzhi Wang, Luqian Weng, G.E.B. Tan, J. Eur. Ceram. Soc. 24 (2004) 825.